

Influence impact of window-size, spatial and radiometric variance, of image bilateral denoising algorithm under AWGN ambience[†]

Vorapoj Patanavijit

Department of Electrical and Electronic Engineering, Vincent Mary School of Engineering,
Assumption University of Thailand, Samuthprakarn 10540, Thailand
E-mail: Patanavijit@yahoo.com

Submitted 30 Dec 2015; accepted in final form 4 January 2017
Available online 29 June 2017

Abstract

Image denoising algorithms are one of the most crucial processes for improving image quality; therefore, a number of denoising algorithms have been proposed. One of the most effective denoising filters is the bilateral filter. The efficiency of the bilateral filter depends on the window size, spatial variance and radiometric variance. In this paper, the impact of the three parameters on the quality of the denoising is investigated. In our experiment, the bilateral filter was applied to suppress the noise of eight standard test images corrupted by five different levels of Gaussian noise. The optimal parameters with regard to the PSNR of the denoised images were then determined.

Keywords: *bilateral filter, denoising algorithm, digital image processing, radiometric variance, window size*

1. Research literature review

In digital image processing (DIP) and digital signal processing, the filter is a crucial and elementary mathematical process (Gonzalez & Woods, 2002). Since 1998, the bilateral filter (BF) (Tomasi & Manduchi, 1998) has been one of the most popular tools for various applications such as noise suppression (Garnett, Huegerich, Chui, & He, 2005; Tomasi & Manduchi, 1998), super resolution (Elad, 2002; Farsiu, Elad, & Milanfar, 2006; Farsiu, Robinson, Elad, & Milanfar, 2004; Wang, Hu, Dong, & Yan, 2013), and video processing (Garnett et al., 2005; Lie, Chen, & Chen, 2011; Lu & Fang, 2013; Shi, Wei, & Pang, 2014). When a bilateral filter is applied, the noise can be effectively removed while the edge or the high frequency component is preserved. There has been a steady improvement on the usage of the bilateral filter. Garnett et al. (2005) proposed the modified bilateral filter, called the trilateral filter, for removing Gaussian noise, impulse noise and the mixture of Gaussian and impulse noise. Lin et al. (2010) integrated the sorted quadrant median vector (SQMV) and the bilateral filter together for removing Gaussian and impulse noise (Lin, Tsai, & Chin, 2010). For the next improvement, Chang et al. (2014) proposed the trilateral filter for removing Rician noise in MR

images (Chang, Hsieh, Tingy, & Chu, 2014). Later, Zhang et al (2011) proposed the bilateral filter for removing speckle noise in SAR images (Zhang, Zhang, & Yang, 2011). In 2011, two groups expanded the usefulness of the bilateral filter for mesh denoising (Zheng, Fu, Au, & Tai, 2011) and preserving image edge in image restoration (Yu, Zhao, & Wang, 2011).

Next, Pinto (Pinto, Costa, Miguel, & Moreira, 2014) implemented the bilateral filtering for image enhancement in surveillance video in 2013 and Wang et al. (2010) implemented trilateral filtering, a modified bilateral filtering, for up-conversion frame rate in video in 2010 (Wang, Zhang, He, & Tan, 2010). Later, Bae (2013) implemented the bilateral filtering for enhancing the infrared small target in 2013. That same year, Hondt et al. (2013) proposed the bilateral filtering for image enhancement in polarimetric SAR image. (Hondt, Guillaso, & Hellwich, 2013). Subsequently, Jung (2013) proposed trilateral filtering for image enhancement in depth map image in 2013. Later, Peng et al. (2014) proposed bilateral filtering for image denoising in multispectral images (Peng, Rao, & Dianat, 2014); and Onuki and Tanaka (Onuki & Tanaka, 2014) proposed trilateral filtering in graph spectral domain. Next, Anantrasirichai et al. (2014)

[†]The Portions of this research work were presented at the IEEE International conference on Advanced Informatics: Concepts, Theory and Application (ICAICTA 2015), Chonburi, Thailand, Aug. 2015, as "The Bilateral Denoising Performance Influence of Window, Spatial and Radiometric Variance", (IEEE Xplore) (Patanavijit, 2015)

proposed the bilateral filtering for image enhancement in optical coherence tomography image. Next two groups proposed the adaptive bilateral filtering for image denoising and speckle denoising. (Yu et al., 2011; Zhang, Tian, & Ren, 2014). In 2014, Lin et al. (Lin, Chen, Kuo, & Lie, 2014) proposed the multi-lateral filter (extended bilateral filtering) with adaptive support-window. Later, Yang (2015), proposed a complete mathematical proof of the bilateral filter in a recursive mathematical framework.

For application of SRR (Super Resolution Reconstruction) algorithms, Elad (2002) first explored a methodical association between bilateral filtering and three other mathematical techniques (robust estimation (RE), anisotropic diffusion (AD), and weighted least squares (WLS)) under the regularized stochastic framework. Later, Farsiu et al. (2004) proposed bilateral filtering for the SRR algorithm based on bilateral regularization and L1 norm. Next, Farsiu et al. (2006) proposed the bilateral filtering for the SRR algorithm based on bilateral regularization and L1 norm in color images. Subsequently, Wang et al. (2013) proposed the SRR algorithm based on trilateral filter (Garnett et al., 2005) (the modified bilateral filter) reconstruction.

For fast computation and real-time applications, Chaudhury et al. (2011) proposed the fast computation technique for bilateral filtering based on trigonometric range kernels (Chaudhury, Sage, & Unser, 2011). Later, Dai et al. (2014) proposed the fast computation technique for Bilateral filtering based on Hermite polynomials (Dai, Yuan, & Zhang, 2014). Subsequently, Gabiger-Rose et al. (2014) implemented the bilateral filter on FPGA for real-time denoising (Gabiger-Rose, Kube, Weigel, & Rose, 2014); and Yang (2014) implemented the bilateral filtering based on efficient hardware for stereo matching in 2014. In 2015, Yang et al. (Yang, Zhao, & Deng, 2015) proposed the fast computation technique for bilateral filtering based on DCT (Discrete Cosine Transform) with a recursive technique; and Chen et al. (2015) proposed the fast trilateral filter (Garnett et al., 2005) based on the adaptive support weight method (Chen, Ardabilian, & Chen, 2015).

For the application of digital video processing, Lie et al. (2011) proposed the trilateral filter for 2D to 3D video conversion based on key-frame propagation (Lie, Chen, & Chen, 2011). Later, Lu and Fang (2013) proposed the trilateral filter (proposed earlier by Garnett et al., 2005) for

motion estimation based on bidirectional motion compensation. Next, Shi et al. (2014) proposed a modified optical flow algorithm the bilateral filter.

For the application on upsampling operation, Yang, et al. (2013) proposed the bilateral filtering for range image upsampling. Next, Jooheok Kim et al. (2014) proposed the bilateral filtering for depth map upsampling (Kim, Jeon, & Jeong, 2014); and Hung and Siu (2012) proposed the bilateral filtering for fast upsampling.

From the literature review, it can be concluded that the bilateral filter is among the most researched filter since 1989. Its performance depends on its three parameters: spatial variance, radiometric variance and window size but each research in this literature sets these bilateral filtering parameters (spatial variance, radiometric variance and window size) for each experiment by using full searching in all possible parameter range and there is no research on the estimation of these bilateral filtering parameters. Hence, this research investigates the effect of the three parameters to the denoising performance and provides the optimal parameter values with regards to the PSNR of denoised images. From the preliminary result (Patanavijit, 2015), which is examined from only three tested images, the optimized range of the three parameter values for each AWGN ambiance can be concluded. Subsequently, when this research is applied on eight standard images and statistical analysis is applied on these results, consequently, the obviously optimized values of the three parameters for each AWGN ambiance can be concluded from extensively simulation experiments for the future implemented propose. The main contribution of this research is not only to reduce the possible parameter range for each AWGN ambiance but also reduce the simulation computation and time consuming because the full searching in all possible parameter range has high computation and time consuming.

2. Philosophy review of bilateral filter

For the additive Gaussian noise, the noisy image \underline{Y} , is the original ideal image \underline{X} , corrupted by the noise, \underline{N} , according to the following equation

$$\underline{Y} = \underline{X} + \underline{N} \quad (1)$$

In 1998, Tomasi and Manduchi introduced the philosophy of bilateral filter, which can be classified as the nonlinear filter for removing Gaussian noise \underline{N} from the noisy signal \underline{Y} whereas

the edge and/or the high-frequency components are preserved.

Initially, the $w(i)$ is delineated as the weighting function for 1-dimensional digital signals or the $w(i, j)$ for 2-dimensional digital signals and the weighting function is constructed for smoothing in regions of identical magnitude (where the $2N + 1$ numbers of pixels are a neighborhood of i) but for leaving the high-frequency components unchanged. In this article, i is delineated as the position of the pixel element under consideration and $\Omega = \Omega_i(N)$ is delineated as the $2N + 1$ neighborhood of i . Next, for the bilateral filter, the weighting function $w(i)$ can be decomposed to the multiplication of the spatial weighting function $w_s(i)$ and radiometric weighting function $w_r(i)$ whereas the $w(i)$, $w_s(i)$ and $w_r(i)$ can be delineated as the following equation

$$w(i) = w_s(i) w_r(i) \quad (1)$$

$$w_s(i) = \exp\left(-|i_0 - i_n|^2 / 2\sigma_s^2\right) \quad (2)$$

$$w_r(i) = \exp\left(-|y(i_0) - y(i_n)|^2 / 2\sigma_r^2\right) \quad (3)$$

where

- i_0 is the location of the pixel element for the filter computation.
- i_n is the location of the neighborhood of that pixel element for the filter computation. ($i_n \in \Omega_i(N)$)
- $y(i_0)$ is the intensity of the pixel element at position i_0 .
- $y(i_n)$ is the intensity of the neighbor pixels.

By this weighting function $w(i)$ or $w_s(i)w_r(i)$, the noisy signal $\hat{x}(i)$ is filtered according to the following equation

$$\hat{x}(i) = \frac{\sum_{n=i-N}^{i+N} w(i) y(i)}{\sum_{n=i-N}^{i+N} w(i)} \quad \text{or} \quad \hat{x}(i) = \frac{\sum_{n=i-N}^{i+N} w_s(i) w_r(i) y(i)}{\sum_{n=i-N}^{i+N} w_s(i) w_r(i)} \quad (4)$$

For the $w_s(i)$ (spatial weighting function), when the spatial difference or the distance between the pixel at i_0 and pixel at i_n increases, the $w_s(i)$ decreases according to the Gaussian function as shown in Eq.(2). The function of $w_s(i)$ is not strictly defined as Gaussian. It can be any nonnegative and zero decreasing functions. However, the original bilateral filter uses Gaussian function for $w_s(i)$. The principle concealing the function of spatial weighting is motivated from that fact that both pixels are contiguous to one another; hence, the intensity value of both pixels should have high association to one another. Conversely, when the displacement between the two pixels is high, their intensities have little association.

For the $w_r(i)$ (radiometric weighting function), when the radiometric difference or the intensity difference between the pixel at i_0 and pixel at i_n increases, the $w_r(i)$ decreases according to Gaussian function as shown in Eq.(3) for the preservation of edges and high frequency components.

For two dimension signals, the computational example of both $w_s(i, j)$ (spatial weighting function) and $w_r(i, j)$ (radiometric weighting function) are shown in Figure1. The filtering processes on the smooth and edge regions are shown in the left and the right subfigures, respectively. From this example, $w_{s,1}(i, j)$ is identical to $w_{s,2}(i, j)$ even though both of the intensities of this pixel group are different. However, $w_{r,1}(i, j)$ and $w_{r,2}(i, j)$ are different due to the different intensity distribution in the neighborhood.

From Eq. (4), the feature of the bilateral filter is managed and defined by three major parameters (N , σ_s and σ_r); therefore, the choosing of N , σ_s and σ_r parameters is crucial, for operating the bilateral filter at the maximum efficiency.

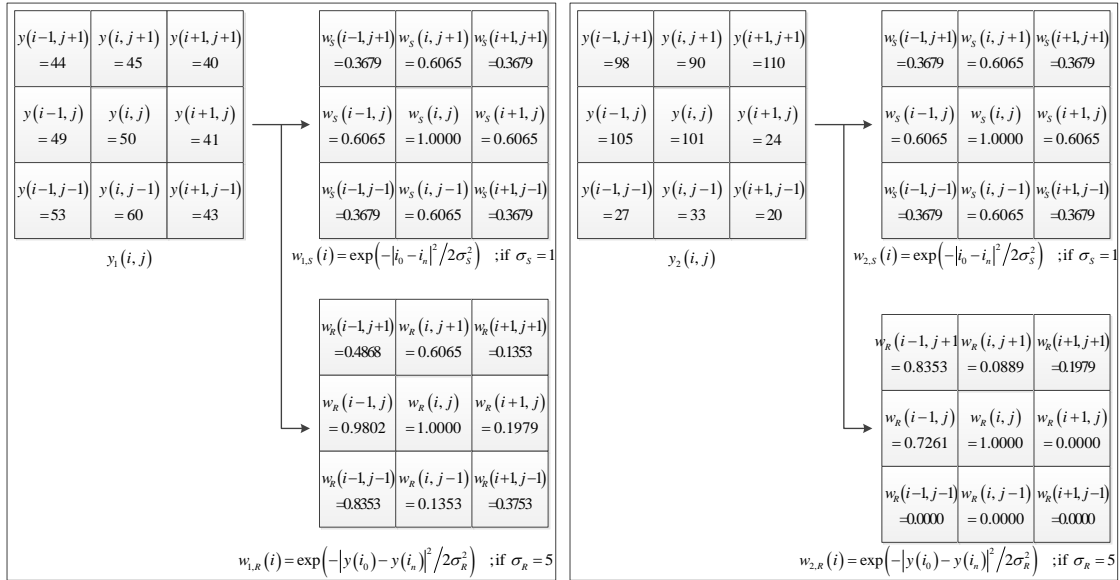


Figure 1 The Computational example of both $w_s(i)$ (spatial weighting function) and the $w_r(i)$ (radiometric weighting function) for a smooth region (left) and an edge region (right)

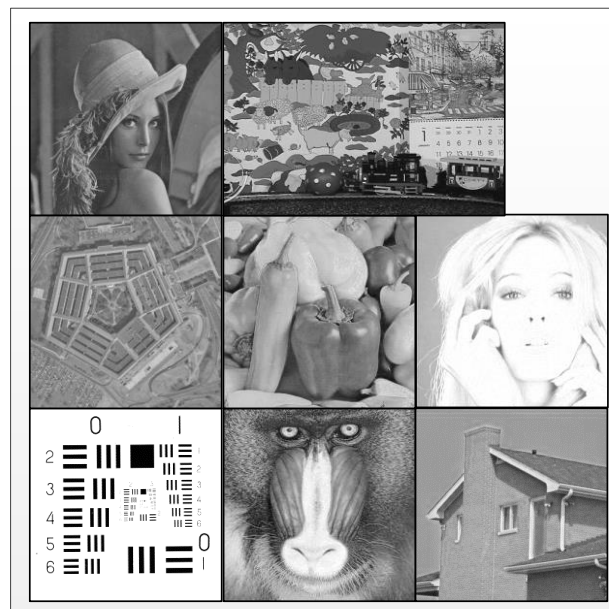


Figure 2 The Original group constitutes of eight standard testing images, from left to right , then down: Lena (256x256), Mobile Frame 10 (352x240), Pentagon (512x512), Peppers (256x256), Girl (Tiffany) (256x256), Resolution (128x128), Baboon (256x256), House (128x128)

3. Impact of N , σ_S and σ_R

The eight standard test images are corrupted by 5 levels of Gaussian noise (SNR = 35dB, 30dB, 25dB, 20dB and 15dB). The test images are Lena (256x256), Mobile Frame 10 (352x240), Pentagon (512x512), Peppers (256x256), Girl (Tiffany) (256x256), Resolution (128x128), Baboon (256x256) and House (128x128). These images (Figure 2) were chosen for investigating the efficient influence consequence of the bilateral filter in image denoising algorithm, which is influenced by three main parameters: window size, spatial variance and radiometric variance. Later, for image denoising purposes, these noisy images were processed by the bilateral filter in order to eradicate and overcome noise for retrieving the original image in all cases.

The PSNR of the filter images is used to measure the performance of the bilateral filter.

3.1 Impact of window size

The objective of this experimental section is to determine the optimal window size, which makes the maximum PSNR therefore the performance, when the window size (N) is set differently, is investigated. Six window sizes (3x3, 5x5, 7x7, 9x9, 11x11 and 21x21) were used in this experiment. σ_S is varied between and including 0.1 to 10.0 with increments of 0.1 and σ_R is varied between and including 0.5 to 60.0 with increments of 0.5. Tables I-VIII show the highest PSNR for the different window sizes at different noise levels. From the results, regarding the PSNR of the denoised image, the optimal window size is either 5x5 or 7x7.

Table 1 The experimental products of window size impact for Lena

LENA SNR (dB)	Window Size					
	3x3	5x5	7x7	9x9	11x11	21x21
15	29.0249	29.6253	29.6376	29.6333	29.6326	29.6325
20	32.4718	32.7607	32.7669	32.7663	32.7662	32.7661
25	35.7103	35.8720	35.8805	35.8810	35.8811	35.8811
30	39.0939	39.1264	39.1272	39.1271	39.1272	39.1272
35	42.8089	42.8819	43.0502	42.8867	43.0502	43.0502

Table 2 The experimental products of window size impact for Mobile

Mobile SNR (dB)	Window Size					
	3x3	5x5	7x7	9x9	11x11	21x21
15	24.4093	24.5900	24.6020	24.6025	24.6025	24.6025
20	28.2548	28.4225	28.4430	28.4449	28.4450	28.4450
25	32.3315	32.4235	32.3315	32.4385	32.4386	32.4386
30	32.4386	36.6758	36.6773	36.6775	36.6775	36.6775
35	41.2157	41.1962	41.2216	41.2016	41.2216	41.2216

Table 3 The experimental products of window size Impact for Pentagon

Pentagon SNR (dB)	Window Size					
	3x3	5x5	7x7	9x9	11x11	21x21
15	26.6205	27.2907	27.2974	27.2884	27.2865	27.2863
20	29.8971	30.0772	30.0672	30.0666	30.0666	30.0666
25	33.2721	33.3753	33.3721	33.3718	30.0666	33.3717
30	36.8274	36.8586	36.8605	36.8606	36.8605	36.0019
35	40.9274	40.9279	40.9279	40.9279	40.9279	40.9279

Table 4 The experimental products of window size impact for Peppers

Pentagon SNR (dB)	Window Size					
	3x3	5x5	7x7	9x9	11x11	21x21
15	26.4238	27.5731	27.6464	27.6270	27.6154	27.6125
20	30.6659	31.0357	31.0463	31.0464	29.6611	29.6538
25	34.0093	34.1143	34.1169	34.1170	34.1170	34.1170
30	37.2741	37.2995	37.2999	37.2999	37.2999	37.2999
35	40.9865	40.9889	40.9889	40.7639	40.9889	40.9889

Table 5 The experimental products of window size impact for Girl (Tiffany)

Pentagon SNR (dB)	Window Size					
	3x3	5x5	7x7	9x9	11x11	21x21
15	22.7640	23.7854	23.9716	23.9647	23.9436	23.9209
20	27.7637	28.2253	28.2479	28.2389	28.2365	28.2360
25	31.7661	32.0321	32.0362	32.0333	32.0327	32.0327
30	37.2741	35.5397	35.5470	35.5468	35.5467	35.5467
35	39.2566	39.3567	39.3654	39.3657	39.3569	39.3569

Table 6 The experimental products of window size impact for Resolution

Pentagon SNR (dB)	Window Size					
	3x3	5x5	7x7	9x9	11x11	21x21
15	20.7602	20.9712	21.0134	21.0232	21.0270	21.0274
20	25.7869	26.0790	26.0173	26.1423	26.1522	26.1524
25	30.7922	31.1407	31.1764	31.2070	31.2195	31.2221
30	35.6976	36.0983	36.1443	36.1711	36.1855	36.1879
35	40.9149	41.3076	41.3833	41.4018	41.3955	41.3971

Table 7 The experimental products of window size impact for Baboon

Pentagon SNR (dB)	Window Size					
	3x3	5x5	7x7	9x9	11x11	21x21
15	24.3077	24.6048	24.6321	24.6343	24.6345	24.6345
20	27.2345	27.5042	27.5116	27.5120	27.5120	27.5120
25	31.1099	31.1151	31.1151	31.1151	31.1151	31.1151
30	35.2914	35.1391	35.1453	35.1531	35.1599	35.1621
35	39.9324	39.9324	39.9324	39.9324	39.9324	39.9324

Table 8 The experimental products of window size impact for House

Pentagon SNR (dB)	Window Size					
	3x3	5x5	7x7	9x9	11x11	21x21
15	26.2516	26.9059	26.9374	26.9382	26.9374	26.9372
20	30.1673	30.5078	30.5303	30.5326	30.5328	30.5328
25	33.7763	34.0650	34.0883	34.0901	34.0901	34.0901
30	37.3987	37.4997	37.5081	37.5082	37.5082	37.5083
35	41.1310	41.2060	41.2130	41.2793	41.2131	41.2132

3.2 Impact of radiometric variance (σ_R)

In this section, the objective of this experimental section is to determine the optimal radiometric variance, which makes the maximum PSNR therefore the effect of σ_R is investigated when the window size is fixed at the optimal sizes 5x5 and 7x7. σ_S is varied between and including 0.1 to 10.0 with increments of 0.1. Note that the graphs in this section show the filter results when σ_S is set such that it provides the highest PSNR for the given σ_R .

3.2.1 Impact of σ_R for the bilateral filter with 5x5 window size

Figures 3.1-3.5 show the highest PSNR for the different σ_R and the window size of 5x5. The noise level is varied for each Figure.

3.2.2 Impact of σ_R for the bilateral filter with 7x7 window size

Figures 4.1-4.5 show the highest PSNR for the different σ_R and the window size of 7x7. The noise level is varied for each Figure.

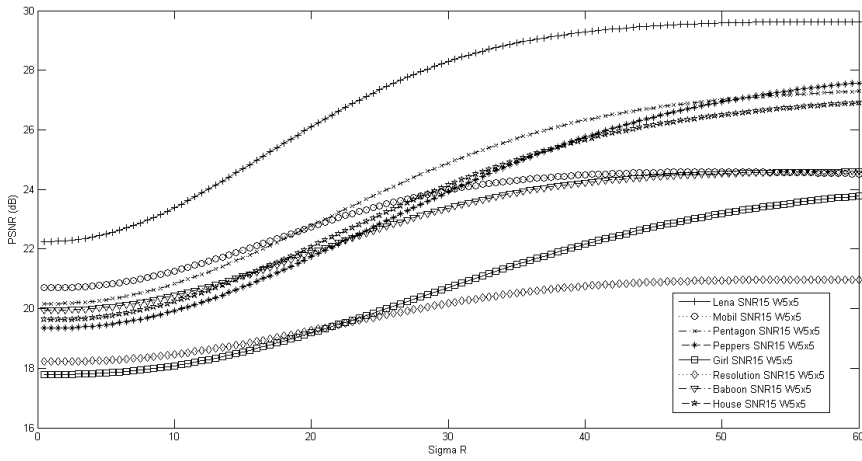


Figure 3.1 Comprehensive investigation consequence of radiometric variance consequence (SNR=15dB)

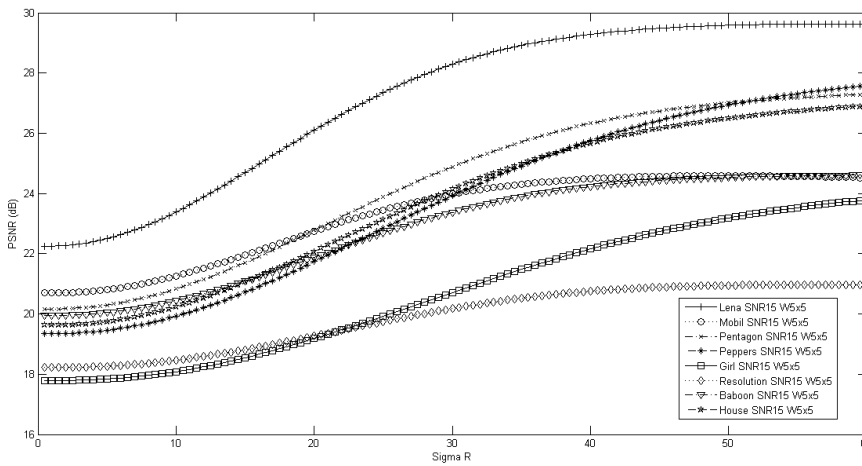


Figure 3.2 Comprehensive investigation sigma consequence of radiometric variance consequence (SNR=20dB)

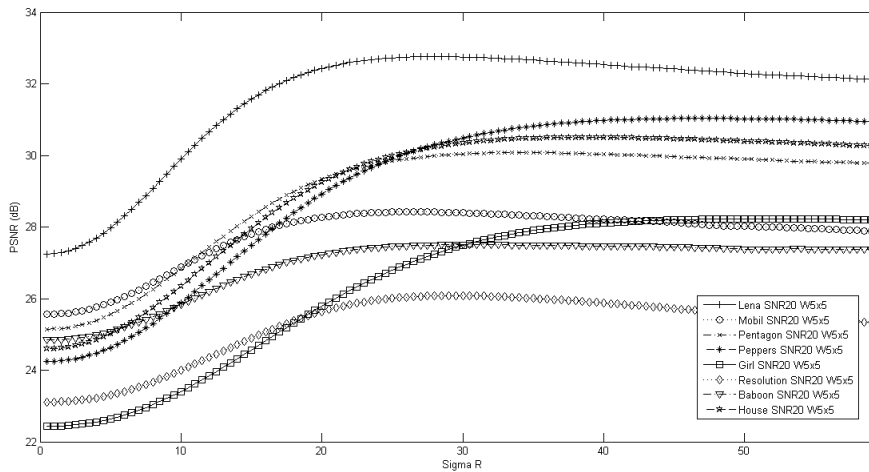


Figure 3.3 Comprehensive investigation consequence of radiometric variance consequence (SNR=25dB)

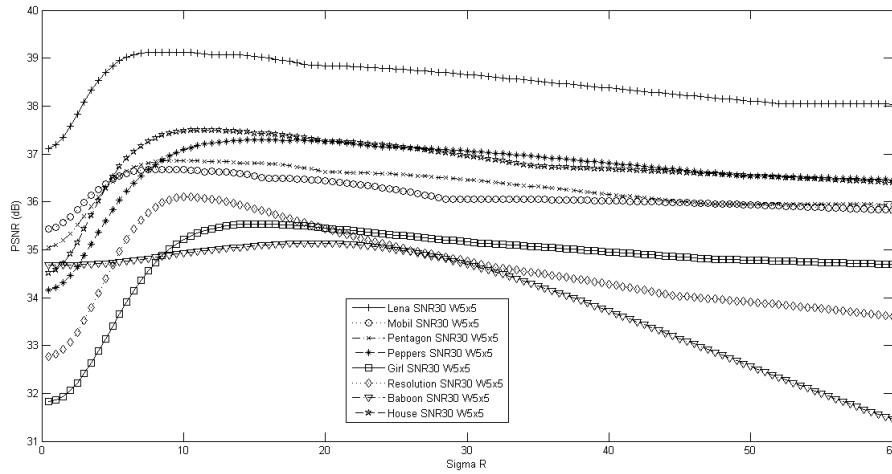


Figure 3.4 Comprehensive investigation consequence of radiometric variance consequence (SNR=30)

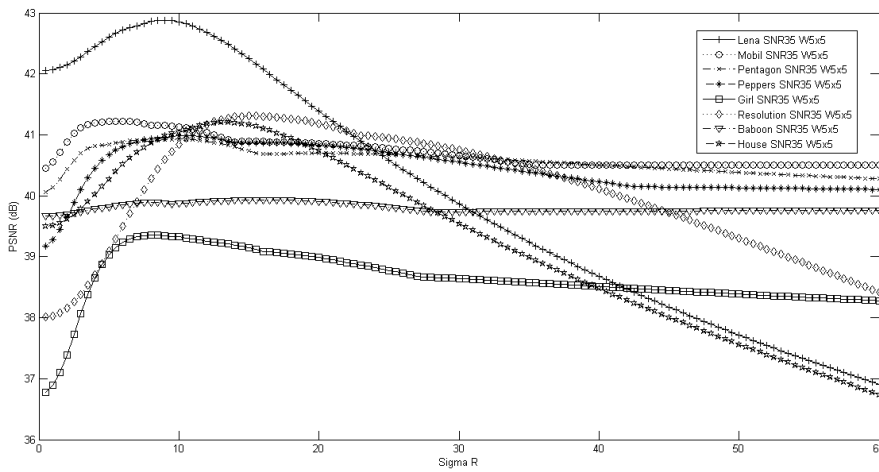


Figure 3.5 Comprehensive investigation consequence of radiometric variance consequence (SNR=35dB)

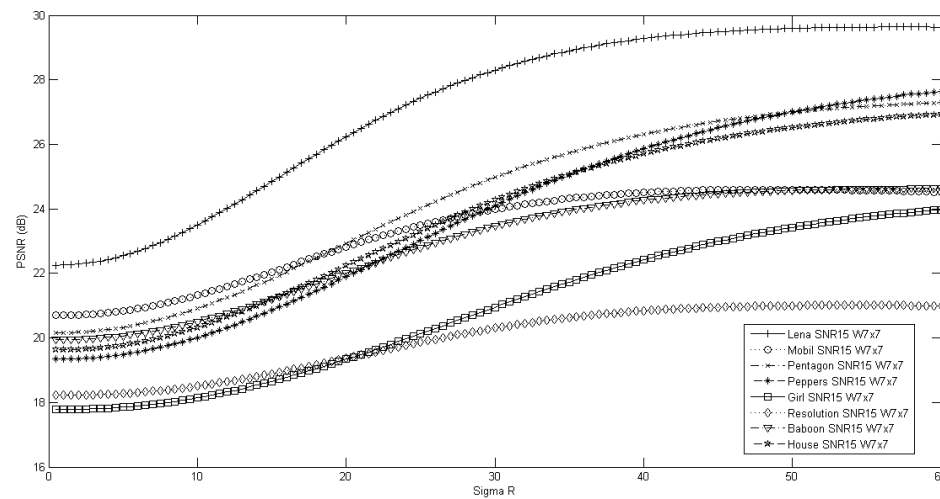


Figure 4.1 Comprehensive investigation consequence of radiometric variance consequence (SNR=15dB)

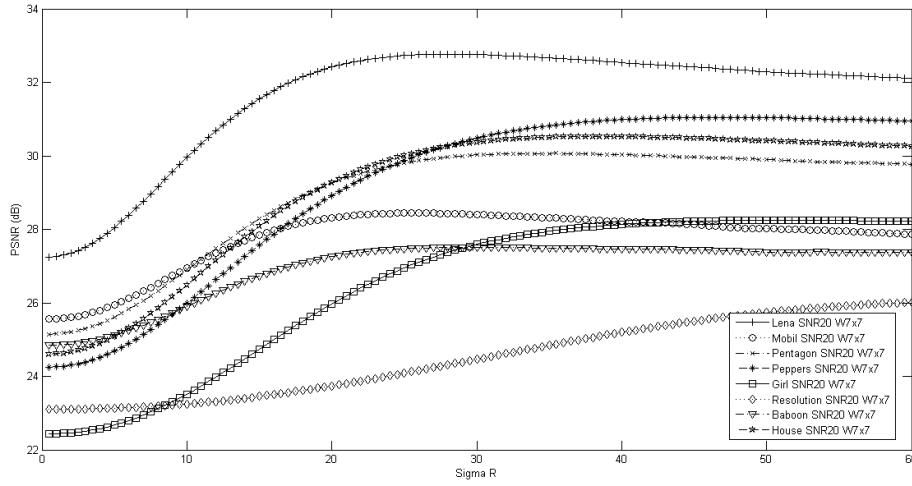


Figure 4.2 Comprehensive investigation consequence of radiometric variance consequence (SNR=20dB)

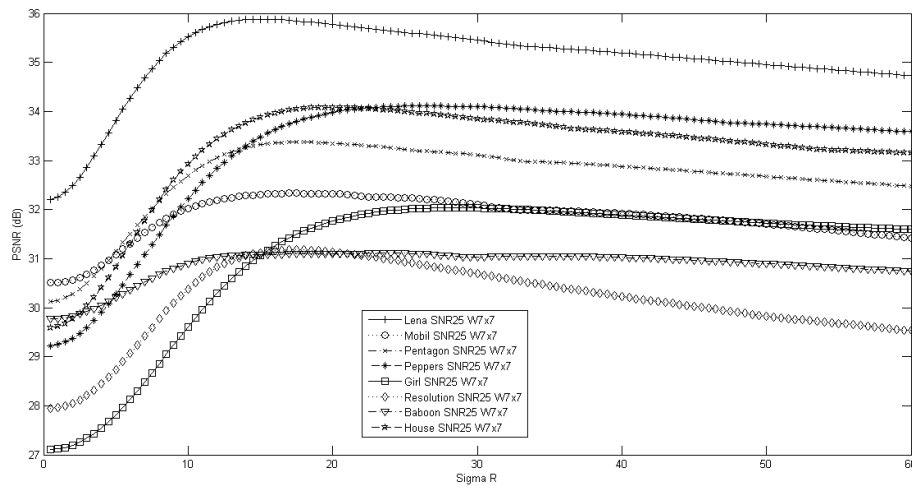


Figure 4.3 Comprehensive investigation consequence of radiometric variance consequence (SNR=25dB)

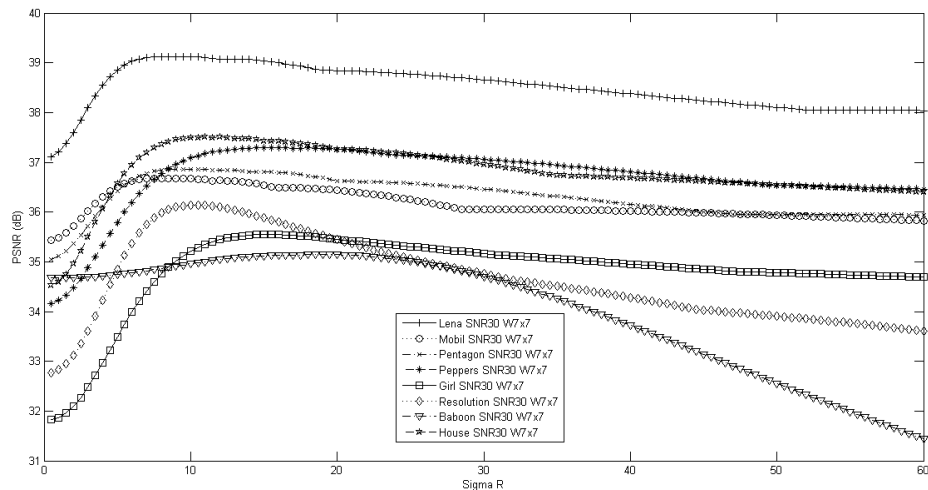


Figure 4.4 Comprehensive investigation consequence of radiometric variance consequence (SNR=30dB)

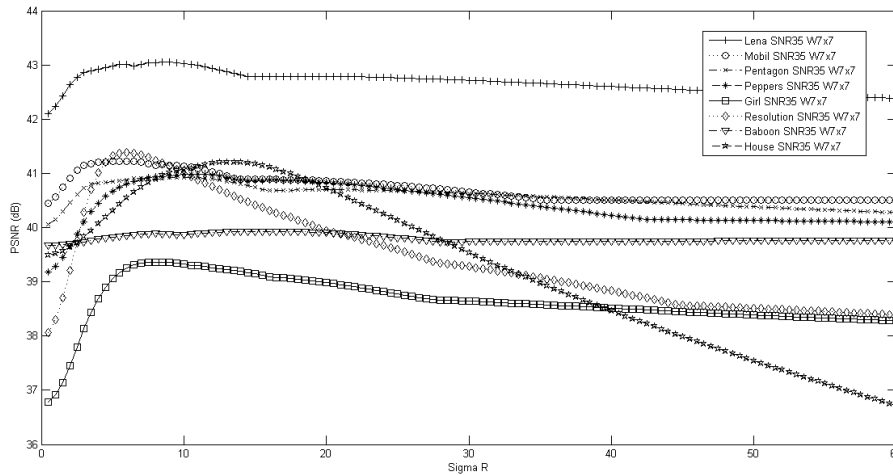


Figure 4.5 Comprehensive investigation consequence of radiometric variance consequence (SNR=35dB)

3.2.3 Discussion

Figures 5.1-5.3 show the relation of σ_s and σ_R providing the highest PSNR for the window size of 5x5, 7x7 and 9x9, respectively. The comparison of the average radiometric variances giving the highest PSNR for different window size is shown in Figure 5.4. From the four figures, it can be concluded that:

- For window size 5x5, the Radiometric Variance, which makes the highest performance (or highest PSNR) is 57.8 ± 3.7 , 35.7 ± 9.3 , 20.4 ± 5.4 , 12.4 ± 3.8 , 10.9 ± 3.6 for noise power at SNR=15dB, 20dB, 25dB, 30dB and 35dB respectively (Figure 5.1).
- For window size 7x7, the Radiometric Variance, which makes the highest performance (or highest PSNR) is 57.4 ± 4.1 , 39.4 ± 12.4 , 20.6 ± 4.8 , 12.1 ± 3.9 , 9.7 ± 3.5 for noise power at SNR=15dB, 20dB, 25dB, 30dB and 35dB respectively (Figure 5.2).
- For window size 9x9, the Radiometric Variance, which makes the highest performance (or highest PSNR) is 57.3 ± 4.2 , 35.4 ± 10.0 , 20.2 ± 5.4 , 15.3 ± 6.0 , 10.4 ± 3.4 for noise power at SNR=15dB, 20dB, 25dB, 30dB and 35dB respectively (Figure 5.3).
- The Radiometric Variance, which makes the highest performance (or highest PSNR), will decrease when the SNR of image increases (or the noise power in that image decreases) as shown in Figure 5.1-5.3. The average value (from three window sizes: 5x5, 7x7 and 9x9) of these Radiometric Variance is 57.5, 36.8, 20.4, 13.3 and 10.3 for noise power at SNR=15dB, 20dB, 25dB, 30dB and 35dB respectively.
- The effect of the window size to the value of σ_R is low. Therefore, the window size should be set to either 5x5 or 7x7 for the highest PSNR (Figure 5.4)

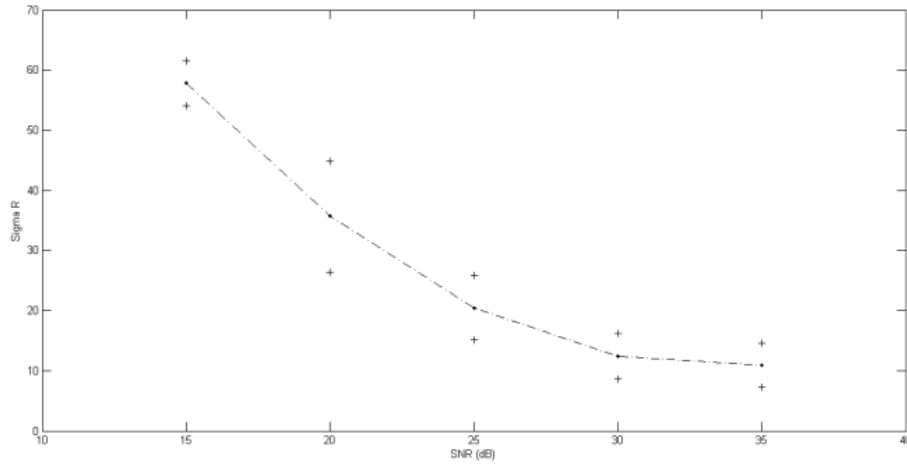


Figure 5.1 The Mean and SD of radiometric variance for maximum PSNR (Window Size 5x5)

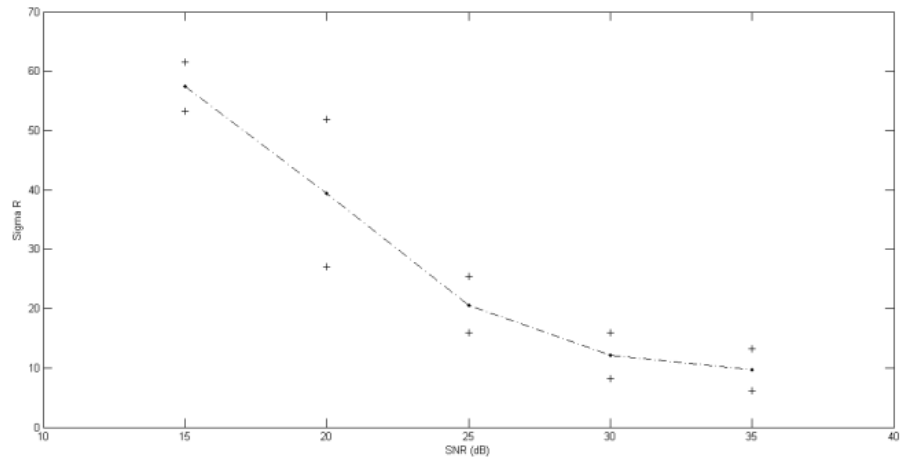


Figure 5.2 The Mean and SD of radiometric variance for maximum PSNR (Window Size 7x7)

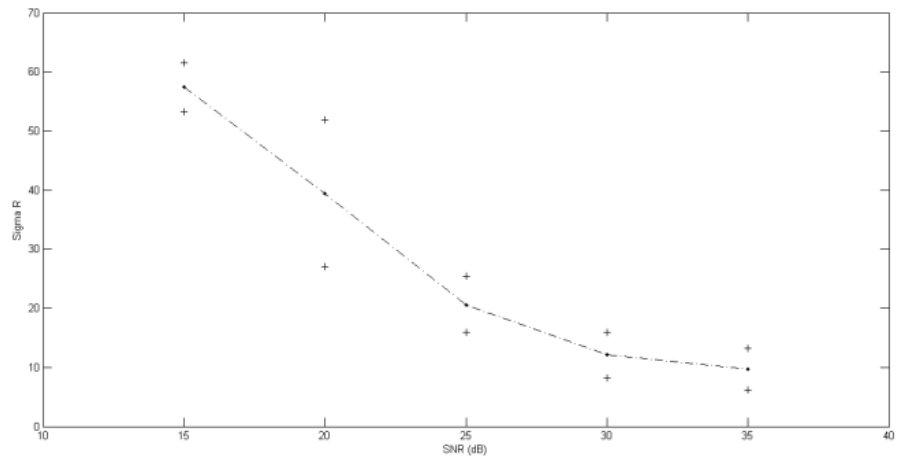


Figure 5.3 The Mean and SD of radiometric variance for maximum PSNR (Window Size 9x9)

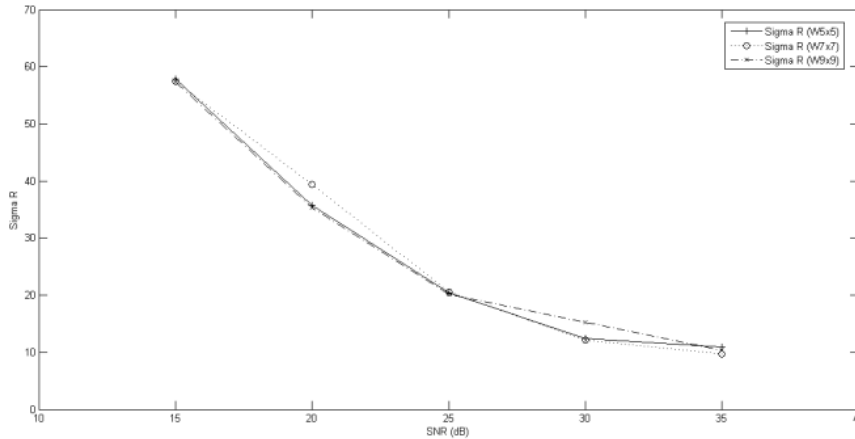


Figure 5.4 The comparison consequence of Mean of radiometric variance for maximum PSNR for three window size (5x5, 7x7 and 9x9)

3.3 Impact of spatial variance (σ_s)

According to Section 3.1, the optimal window size is either 5x5 or 7x7. In this section, the objective of this experimental section is to determine the optimal spatial variance, which makes the maximum PSNR therefore the effect of σ_s is investigated when the window size is fixed at 5x5 and 7x7. σ_R is varied between and 0.5 to 60.0 with increments of 0.5. Note that the graphs in this section show the filter result when σ_s is set such that it provides the highest PSNR for the given σ_R .

3.3.1 Impact of σ_s for the bilateral filter with 5x5 window size

Figures 6.1-6.5 show the highest PSNR for the different σ_s and the window size of 5x5. The noise level is varied for each figure.

3.3.2 Impact of σ_s for the bilateral filter with 7x7 window size

Figure 7.1-7.5 shows the highest PSNR for the different σ_s and the window size of 7x7. The noise level is varied for each figure.

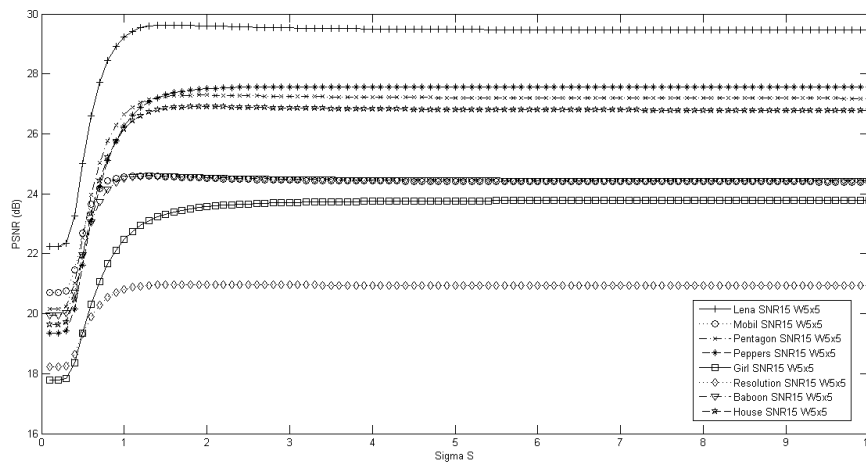


Figure 6.1 Comprehensive investigation consequence of spatial variance consequence (SNR=15dB)

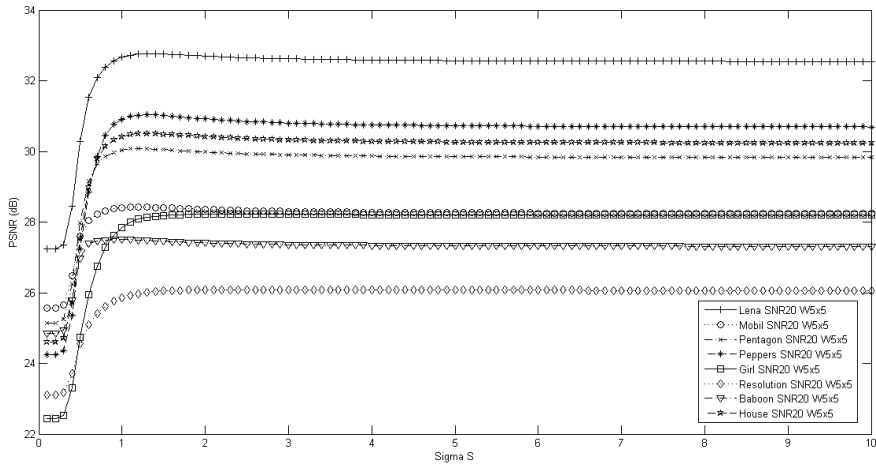


Figure 6.2 Comprehensive investigation consequence of spatial variance consequence (SNR=20dB)

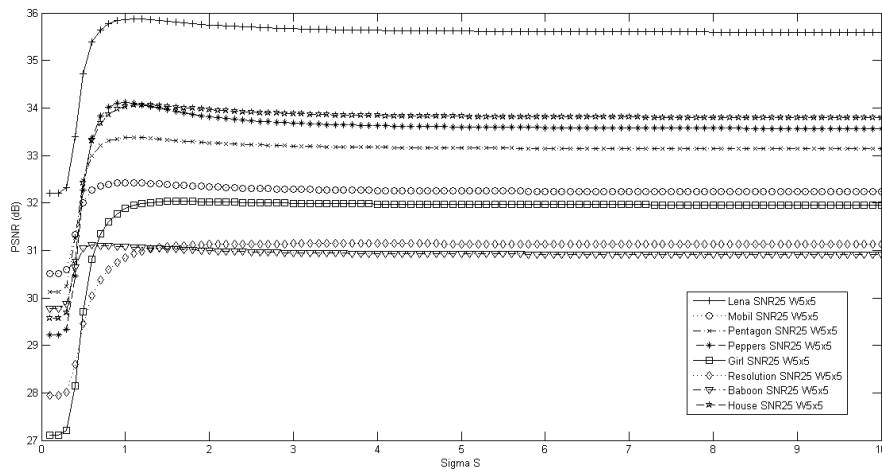


Figure 6.3 Comprehensive investigation consequence of spatial variance consequence (SNR=25dB)

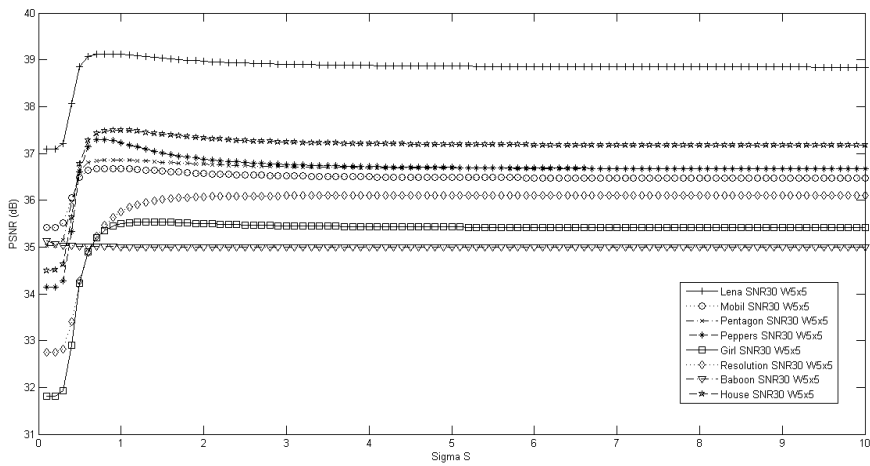


Figure 6.4 Comprehensive investigation consequence of spatial variance consequence (SNR=30dB)

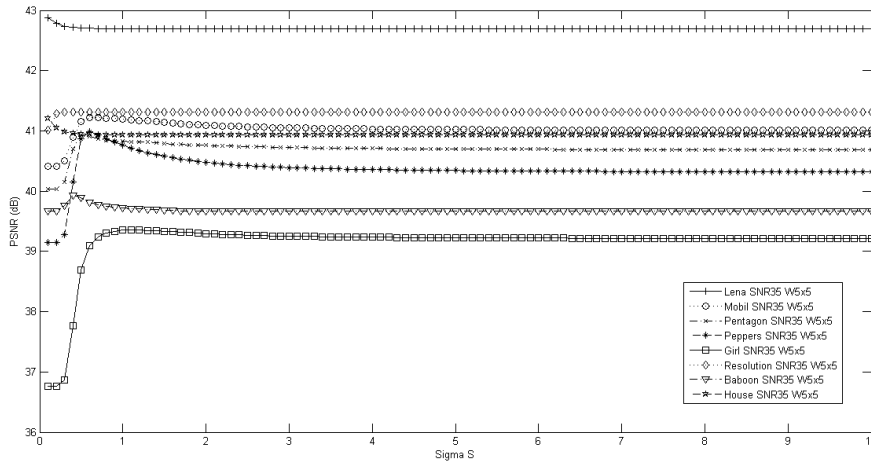


Figure 6.5 Comprehensive investigation consequence of spatial variance consequence (SNR=35dB)

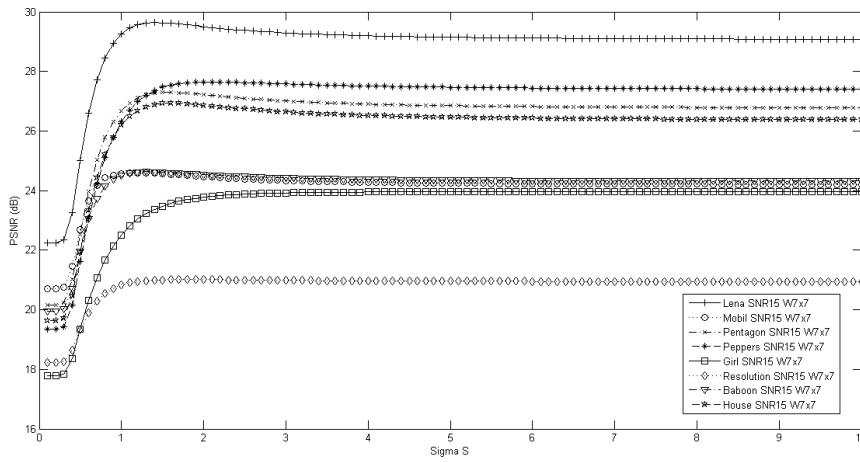


Figure 7.1 Comprehensive investigation consequence of spatial variance consequence (SNR=15dB)

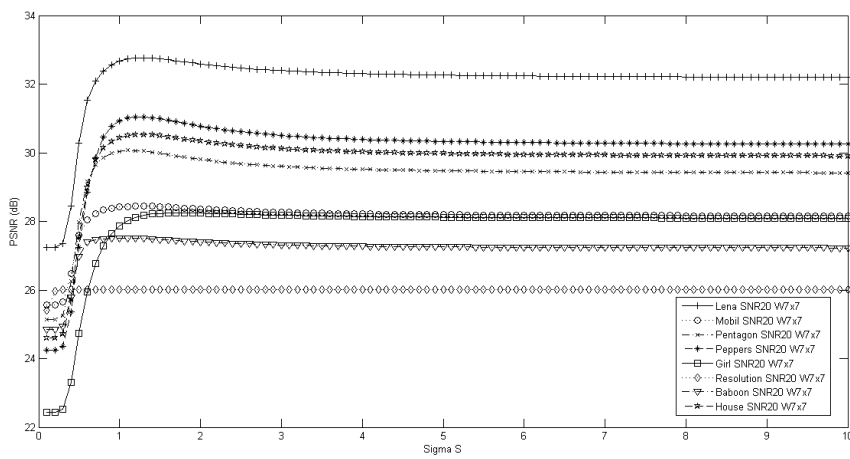


Figure 7.2 Comprehensive investigation consequence of spatial variance consequence (SNR=20dB)

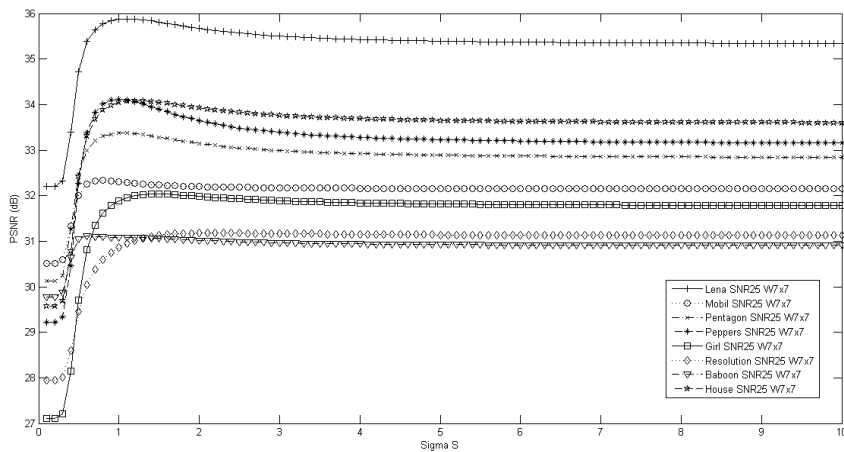


Figure 7.3 Comprehensive investigation consequence of spatial variance consequence (SNR=25dB)

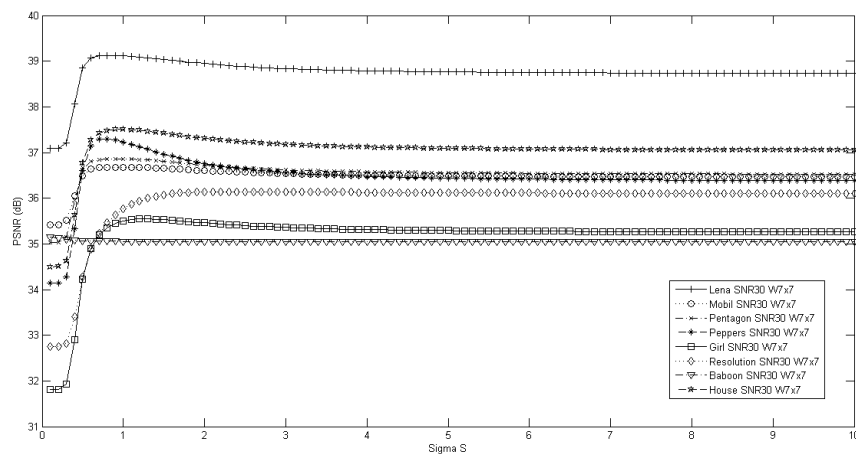


Figure 7.4 Comprehensive investigation consequence of spatial variance consequence (SNR=30dB)

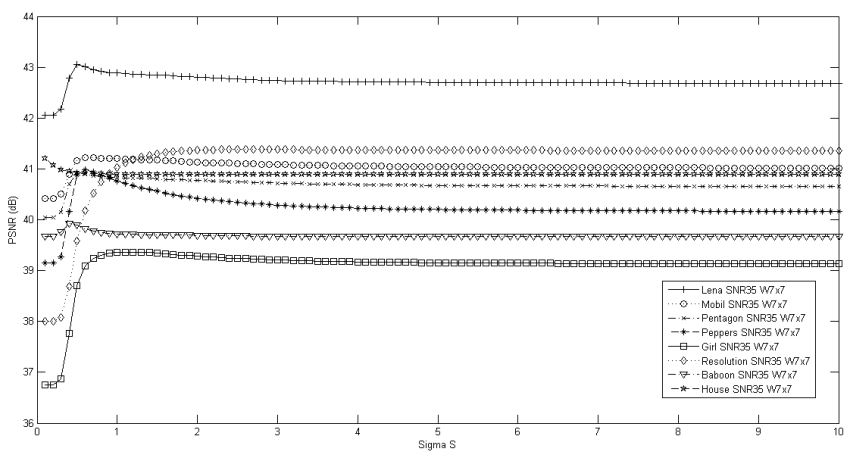


Figure 7.5 Comprehensive investigation consequence of spatial variance consequence (SNR=35dB)

3.3.3 Discussion

Figures 8.1-8.3 show the relation of σ_s and σ_R providing the highest PSNR for the window size of 5x5, 7x7 and 9x9, respectively. The comparison of the average radiometric variances giving the highest PSNR for different window size is shown in Figure 8.4. From the four Figures, it can be concluded that:

- For window size 5x5, the Spatial Variance, which makes the highest performance (or highest PSNR) is 2.9 ± 3.0 , 1.5 ± 0.5 , 1.4 ± 0.9 , 1.2 ± 1.2 , 0.5 ± 0.4 for noise power at SNR=15dB, 20dB, 25dB, 30dB and 35dB respectively (Figure 8.1).
- For window size 7x7, the Spatial Variance, which makes the highest performance (or highest PSNR) is 2.6 ± 3.0 , 1.2 ± 0.4 , 1.1 ± 0.6 , 1.0 ± 0.6 , 0.8 ± 0.8 for noise power at SNR=15dB, 20dB, 25dB, 30dB and 35dB respectively (Figure 8.2).
- For window size 9x9, the Spatial Variance, which makes the highest performance (or highest PSNR) is 2.6 ± 3.0 , 1.4 ± 0.3 , 1.2 ± 0.5 , 0.7 ± 0.4 , 0.7 ± 0.8 for noise power at SNR=15dB, 20dB, 25dB, 30dB and 35dB respectively (Figure 8.3).
- The Spatial Variance, which makes the highest performance (or highest PSNR), will decrease when the SNR of image increases (or the noise power in that image decreases) as shown in Figure 8.1-8.3. The average value (from three window sizes: 5x5, 7x7 and 9x9) of these Spatial Variance is 2.7, 1.3, 1.2, 1.0, 0.7 for noise power at SNR=15dB, 20dB, 25dB, 30dB and 35dB respectively.
- The effect of the window size to the value of σ_s is low. Therefore, the window size should be set to either 5x5 or 7x7 for the highest PSNR (Figure 8.4)

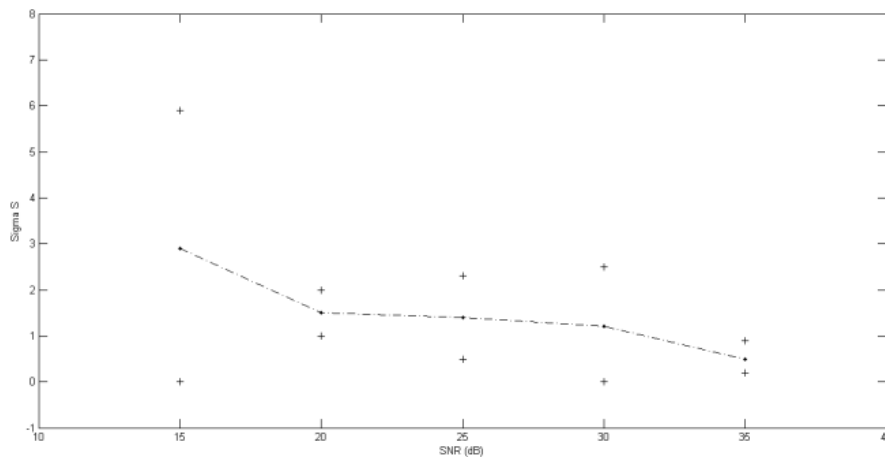


Figure 8.1 The Mean and SD of spatial variance for maximum PSNR (Window Size 5x5)

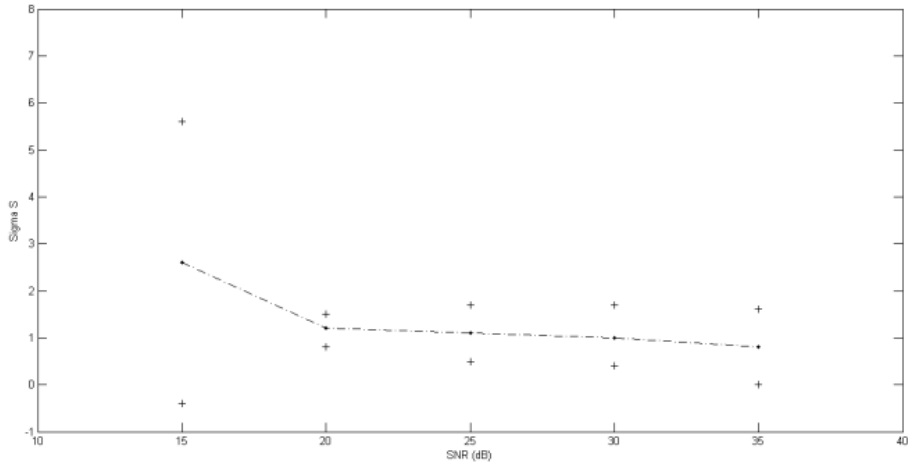


Figure 8.2 The Mean and SD of spatial variance for maximum PSNR (Window Size 7x7)

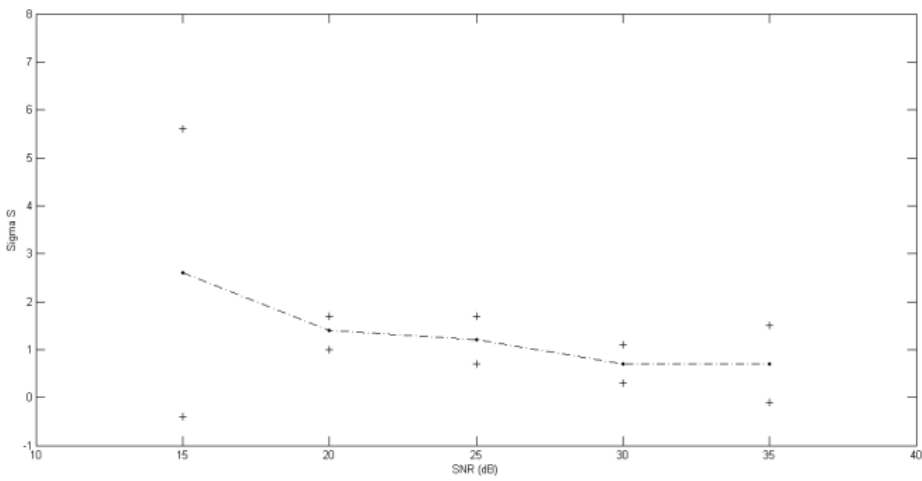


Figure 8.3 The Mean and SD of spatial variance for maximum PSNR (Window Size 9x9)

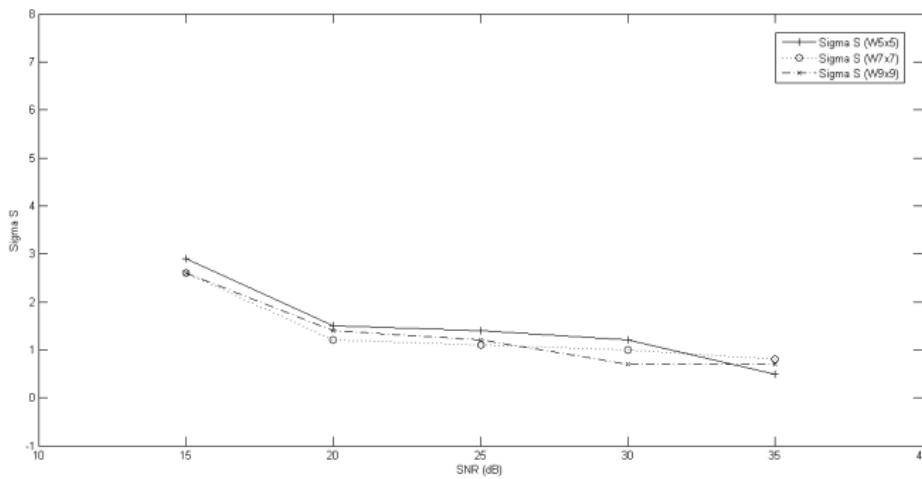


Figure 8.4 The comparison consequence of Mean of spatial variance for maximum PSNR for three window size (5x5, 7x7 and 9x9)

4. Conclusion

In this article, the impact of the window size, spatial and radiometric variances to the denoising performance of a bilateral filter is investigated. The experiment on denoising eight Gaussian-noise corrupted images was performed to find the optimal values of the three parameters at different noise levels. In addition, an experimental setting value of three major parameters: window size (in section 3.1), spatial variance (in section 3.2.3) and radiometric variance (in section 3.3.3), which generates the denoised images with the maximum PSNR measurement, are thoroughly studied for each case of all eight tested images and all five noise environments.

5. Acknowledgement

The research project was funded by Assumption University.

6. References

- Anantrasirichai, N., Nicholson, L., Morgan, J. E., Erchova, I., Mortlock, K., North, R. V., . . . Achim, A. (2014). Adaptive-weighted bilateral filtering and other pre-processing techniques for optical coherence tomography. *Computerized Medical Imaging and Graphics*, 38(6), 526-539. <https://doi.org/10.1016/j.compmedimag.2014.06.012>
- Bae, T.-W. (2013). Spatial and temporal bilateral filter for infrared small target enhancement, *Infrared Physics & Technology*, 63, 42-53. DOI: 10.1016/j.infrared.2013.12.007
- Chang, H., Hsiehy, T., Tingy, Y., & Chu, W. (2014). Rician noise removal in MR images using an adaptive trilateral filter. *International Conference on Biomedical Engineering and Informatics (BMEI)*. Pages 467-471. Doi: 10.1109/BMEI.2011.6098281
- Chaudhury, K. N., Sage, D., & Unser, M. (2011). Fast O(1) bilateral filtering using trigonometric range kernels. *IEEE Transactions on Image Processing*, 20(12), 3376-3382. DOI: 10.1109/TIP.2011.2159234
- Chen, D., Ardabilian, M., & Chen, L. (2015). A fast trilateral filter-based adaptive support weight method for stereo matching. *IEEE Transactions on Circuits and Systems for Video Technology*, 25(5), 730-743. DOI: 10.1109/TCSVT.2014.2361422
- Dai, L., Yuan, M., & Zhang, X. (2014). Accelerate bilateral filter using Hermite polynomials. *Electronics Letters*, 50(20), 1432-1434. DOI: 10.1049/el.2014.2758
- Elad, M. (2002). On the origin of the bilateral filter and ways to improve it. *IEEE Transactions on Image Processing*, 11(10), 1141-1151. DOI: 10.1109/TIP.2002.801126.
- Farsiu, S., Elad, M., & Milanfar, P. (2006). Multiframe demosaicing and super-resolution of color images. *IEEE Transactions on Image Processing*, 15(1), 141-159. DOI: 10.1109/TIP.2005.860336
- Farsiu, S., Robinson, M. D., Elad, M., & Milanfar, P. (2004). Fast and robust multiframe super resolution. *IEEE Transactions on Image Processing*, 13(10), 1327-1344.
- Gabiger-Rose, A., Kube, M., Weigel, R., & Rose, R. (2014). An FPGA-based fully synchronized design of a bilateral filter for real-time image denoising. *IEEE Transactions on Industrial Electronics*, 61(8), 4093-4104. DOI: 10.1109/TIE.2013.2284133
- Garnett, R., Huegerich, T., Chui, C., & He, W. (2005). A universal noise removal algorithm with an impulse detector. *IEEE Transactions on Image Processing*, 14(11), 1747-1754.
- Gonzalez, R. C., & Woods, R. E. (2002). *Digital image processing* (2nd ed.). Upper Saddle River, NJ, USA: Prentice-Hall.
- Hondt, O. D., Guillaso, S., & Hellwich, O. (2013). Iterative bilateral filtering of polarimetric SAR data. *IEEE Journal of Selected Topics in Applied Earth Observations and Remote Sensing*, 6(3), 1628-1639. DOI: 10.1109/JSTARS.2013.2256881
- Hung, K.-W., & Siu, W.-C. (2012). Fast image interpolation using the bilateral filter. *IET Image Process*, 6(7), 877-890. DOI: 10.1049/iet-ipr.2011.0050
- Jung, S.-W. (2013). Enhancement of image and depth map using adaptive joint trilateral filter. *IEEE Transactions on Circuits and Systems for Video Technology*, 23(2),

- 258-269. DOI:
10.1109/TCSVT.2012.2203734
- Kim, J., Jeon, G., & Jeong, J. (2014). Joint-adaptive bilateral depth map upsampling. *Signal Processing: Image Communication*, 29(4), 506-513. <https://doi.org/10.1016/j.image.2014.01.011>
- Lie, W.-N., Chen, C.-Y., & Chen, W.-C. (2011). 2D to 3D video conversion with key-frame depth propagation and trilateral filtering. *Electronics Letters*, 47(5), 319-321. DOI: 10.1049/el.2010.2912
- Lin, G., Chen, C., Kuo, C., & Lie, W. (2014). A computing framework of adaptive support-window multi-lateral filter for image and depth processing. *IEEE Transactions on Broadcasting*, 60(3), 452-463. DOI: 10.1109/TBC.2014.2330391
- Lin, C., Tsai, J., & Chiu, C. (2010). Switching bilateral filter with a texture/noise detector for universal noise removal. *IEEE Transactions on Image Processing*, 19(9), 2307-2320. DOI: 10.1109/TIP.2010.2047906
- Lu, Q., & Fang, X. (2013). Joint trilateral motion vector filter for bidirectional motion compensation. *Electronics Letters*, 49(13), 798-800. DOI: 10.1049/el.2013.0995
- Onuki, M., & Tanaka, Y. (2014). Trilateral filter on graph spectral domain, *IEEE International Conference on Image Processing (ICIP 2014)*. pp. 2046-2050.
- Patanavijit, V. (2015). The bilateral denoising performance influence of window, spatial and radiometric variance. *The IEEE International conference on Advanced Informatics: Concepts, Theory and Application (ICAICTA 2015)*, Chonburi, Thailand. pp. 1-6.
- Peng, H., Rao, R., & Dianat, S. A. (2014). Multispectral image denoising with optimized vector bilateral filter. *IEEE Transactions on Image Processing*, 23(1), 264-273. DOI: 10.1109/TIP.2013.2287612
- Pinto, A. M., Costa, P. G., Miguel, V. C., & Moreira, A. P. (2014). Enhancing dynamic videos for surveillance and robotic applications: the robust bilateral and temporal filter. *Signal Processing: Image Communication*, 29(1), 80-95. <https://doi.org/10.1016/j.image.2013.11.003>
- Shi, B., Wei, J., & Pang, M. (2014). A modified optical flow algorithm based on bilateral-filter and multi-resolution analysis for PIV image processing, *Journal of Flow Measurement and Instrumentation*, 38, 121-130. DOI: 10.1016/j.flowmeasinst.2014.05.005
- Tomasi, C., & Manduchi, R. (1998). Bilateral filtering for gray and color images, *Proceedings of the 1998 IEEE International Conference on Computer Vision*, Bombay, India. pp. 839-846.
- Wang, S., Hu, B., Dong, X., & Yan, X. (2013). An improved super-resolution reconstruction algorithm based on regularization. *ISCC-C '13 Proceedings of the 2013 International Conference on Information Science and Cloud Computing Companion*. pp. 716-721. DOI: 10.1109/ISCC-C.2013.44
- Wang, C., Zhang, L., He, Y., & Tan, Y. (2010). Frame rate up-conversion using trilateral filtering. *IEEE Transactions on Circuits and Systems for Video Technology* 20(6), 886-893. DOI: 10.1109/TCSVT.2010.2046057
- Yang, Q. (2014). Hardware-efficient bilateral filtering for stereo matching. *IEEE Transactions on Pattern Analysis and Machine Intelligence*, 36(5), 1026-1032. DOI: 10.1109/TPAMI.2013.186
- Yang, Q. (2015). Recursive approximation of the bilateral filter. *IEEE Transactions on Image Processing*, 24(6), 1919-1927. DOI: 10.1109/TIP.2015.2403238
- Yang, Q., Ahuja, N., Yang, R., Tan, K.-H., Davis, J., Culbertson, B., . . . Wang, G. (2013). Fusion of median and bilateral filtering for range image upsampling. *IEEE Transactions on Image Processing*, 22(12), 4841-4852. DOI: 10.1109/TIP.2013.2278917
- Yang, K., Zhao, Y., & Deng, N. (2015). Fast bilateral filtering using the discrete cosine transform and the recursive method. *Optik - International Journal for Light and Electron Optics*, 126(6), 592-595. <https://doi.org/10.1016/j.ijleo.2015.01.025>

- Yu, Y., Dong, G., & Wang, J. (2011). Despeckling trilateral filter. *IEEE Workshop on IVMSP 2011*. pp. 42-47. DOI: 10.1109/IVMSPW.2011.5970352
- Yu, H., Zhao, L., & Wang, H. (2011). An efficient edge-based bilateral filter for restoring real noisy image. *IEEE Transactions on Consumer Electronics*, 57(2), 682-686.
- Zheng, Y., Fu, H., Au, O. K.-C., & Tai, C.-L. (2011). Bilateral normal filtering for mesh denoising. *IEEE Transactions on Visualization and Computer Graphics*, 17(10), 1521-1532. DOI: 10.1109/TVCG.2010.264
- Zhang, Y., Tian, X., & Ren, P. (2014). An adaptive bilateral filter based framework for image denoising. *Neurocomputing*, 140(1), 299-316(18).
- Zhang, W. G., Zhang, Q., & Yang, C. S. (2011). Improved bilateral filtering for SAR image despeckling. *Electronics Letters*, 47(4), 286-288. DOI: 10.1049/el.2010.2982